Asian Journal of Chemistry; Vol. 36, No. 7 (2024), 1609-1619

ASIAN JOURNAL OF CHEMISTRY

https://doi.org/10.14233/ajchem.2024.31430

In silico Analysis of Antiviral Potential of New Coumarin Analogues against Coronavirus

MOHAMMAD AUWAL SA'AD[1,2], MANICKAM RAVICHANDRAN[1], SHIVKANYA FULORIA[3,*], LALITHA PATTABHIRAMAN[4], VEERASAMY RAVICHANDRAN[3], FAIZUL FIKRI MOHD YUSOP[5] and NEERAJ KUMAR FULORIA[3,*]

[1]Department of Biotechnology, Faculty of Applied Science, AIMST University, Bedong 08100, Kedah, Malaysia
[2]Centre of Excellence for Vaccine Development (CoEVD), Faculty of Applied Science, AIMST University, Bedong 08100, Kedah, Malaysia
[3]Faculty of Pharmacy, AIMST University, Bedong Kedah, Malaysia
[4]Faculty of Medicine, AIMST University, Bedong Kedah, Malaysia
[5]Veterinary Research Institute (VRI), Ipoh 31350, Malaysia

*Corresponding authors: E-mail: shivkanya_fuloria@aimst.edu.my; nfuloria@aimst.edu.my

Received: 23 February 2024; *Accepted*: 24 May 2024; *Published online*: 29 June 2024; AJC-21681

In silico designing of new chemical moieties to develop as active therapeutic agents is a continuous process. COVID-19 pandemic realized coronaviruses to pose significant global health threat. Current study presents *in silico* antiviral potential of novel coumarin analogues (NCAs) against coronaviruses through molecular docking analysis (MDA) and quantitative structure-activity relationship (QSAR) analysis. This study explores the binding affinity and structure-activity relationships of NCAs, focusing on their interaction with the SARS-CoV-2 spike protein *N*-terminal domain. MDA, particularly highlighting compound **5e**, suggests promising binding interactions. Additionally, the QSAR studies identified key molecular descriptors influencing coronavirus inhibition activity and cytotoxicity (CC_{50}), leading to the development of robust QSAR models meeting OECD criteria. These models demonstrate the stability, validity and applicability of NCAs as potential antiviral agents against coronaviruses. The promising result of new coumarin analogues provides a foundation for the development of novel therapeutics aimed to combat coronaviruses.

Keywords: Coronaviruses, SARS-CoV-2, Coumarin, QSAR, Molecular docking.

INTRODUCTION

Coumarin derivatives have attracted attention in recent years due to their diverse pharmacological properties, including antiviral activity [1,2]. Coumarin is an oxygenated heterocyclic compound having diverse biological properties, which include antiviral activity [3]. Due to the recent COVID outbreak, coumarin gained attention in anti-SARS-CoV-2 drug development. Several studies have conducted *in silico* evaluation of coumarin derivatives to determine their antiviral activity against SARS-CoV-2. A study evaluated coumarin derivatives as potential inhibitors of coronaviruses $3CL^{pro}$, a chymotrypsin-like protease by *in silico* approaches, the MDA results suggested more than half of the coumarin phytochemicals had favourable interaction at the binding pocket of the coronaviruses $3CL^{pro}$ and exhibited better binding affinities toward $3CL^{pro}$ than ritonavir and lopinavir [4]. Another study reported that the coumarin derivatives have a stable binding affinity when docked against different proteins (Spike S1-subunit, NSP5, NSP12, NSP15 and NSP16) of the SARS-CoV-2.

The molecular docking analysis (MDA) results further revealed that three of the coumarin derivatives have a better binding affinity compared to hydroxychloroquine, favipiravir and warfarin, but lower than the binding affinity of remdesivir [5]. Similarly, another *in silico* study approach revealed that three coumarin derivatives exhibit binding affinity towards the M^{pro} protein of SARS-CoV-2 better than cinanserin and chloroquine. All of the investigated compounds bind to the active position of the mentioned protein [6]. Virtual drug screening and molecular docking analysis (MDA) against nucleocapsid and NTD of SARS-CoV-1, SARS-CoV-2, MERS-CoV, HCoV-OC43, HCoV-NL63, HCoV-229E and HCoV-HKU1 revealed good binding affinity to coumarin derivatives while showing low cytotoxicity against human A549 and MRC-5 cell lines [7]. RNA-dependent RNA polymerase (RdRp) of the SARS-CoV-2 virus is one of the key targets that are involved in viral genome replication.

A recent study evaluated the *in silico* antiviral potential of benzophenone-coumarin derivatives (BCDs) against this protein target. The *in silico* analysis resulted in BCD-8 showing an extensive molecular interaction in comparison with that of the standard control used (remdesivir). The drug likeliness and pharmacokinetic analyses also proved the efficiency of BCD-8 as an effective drug without adverse effects [8]. Despite the promising activities of coumarin derivatives, their specific efficacy against coronaviruses and the underlying mechanism of action remains largely unexplored [9]. Hence, the present study was intended to provide valuable insights into the interactions between novel coumarin analogues (NCAs) and viral targets, particularly focusing on the SARS-CoV-2 spike protein *N*-terminal domain. By exploring the promising properties of coumarin derivatives and applying advanced computational methods, this research seeks to identify promising candidates for further preclinical and clinical investigations.

EXPERIMENTAL

Molecular docking analysis: In present study, a MDA of designed molecules was carried out to assess the interaction and binding mode with the target receptor/enzyme using Autodock vina. The structures of all tested compounds were modelled using the Chemsketch software. The structures were optimized and energy was minimized using the auto dock software [10, 11]. The optimized compounds were used to perform MDA and the 3D structures of the molecular target were obtained from Protein Data Bank (PDB): SARS-CoV-2 spike protein N-terminal domain (7B62), SARS-CoV-2 nucleocapsid protein C-terminal domain (7UXZ), the co-crystal structure of SARS-CoV-2 main protease (7DGB), SARS-CoV-2 3CL protease (7P35). The steps for receptor preparation included the removal of heteroatoms (water and ions), the addition of polar hydrogen and the assignment of charge. The active sites were defined using grid boxes of appropriate sizes around the bound cocrystal ligands. The MDA was performed using Auto Dock Vina and Chimera for visualization [12]. The docked pose of ligands and their interactions were analyzed after the end of MDA.

Design of compounds: The designed NCAs included ester, hydrazide, imino, thiazolidinone, and oxadiazole group in the coumarin moiety, which are generally synthesized based on incorporation of ester group on treatment with ethylchloroacetate [13], by incorporating of hydrazide group on treatment with hydrazine hydrate [14], by incorporating imino group through Schiff reaction using various aromatic aldehydes [15], by incorporating of thiazolidinone group through cyclization reaction using thioglycolic acid [16] and by incorporating oxadiazole group (through cyclization reaction using various aromatic acids), respectively [17].

2D-QSAR

Data collection: The coronavirus inhibition activity and cytotoxicity (CC_{50}) of 18 novel coumarin analogues (NCAs) were applied as dependent variables which were expressed with $pIC_{50} = -\log_{10}IC_{50}$. Software of PaDEL-descriptor was applied to determine the molecular descriptors. The NCAs structures were built using ChemDraw Cambridge software and statistics was applied using QSARINS. Designed structures were saved into molfiles, followed by uploading into PaDEL. In total, 1,000 MDs were determined and saved in CSV files.

2D QSAR analysis: Data was pre-treated for MDs after normalizing to eliminate redundant data (high correlation MDs with $r^2 > 0.85$) and constant value (noise); thereby MDs reduce to 4000. QSARINS was used to develop model of 2D QSAR applying MLR process [18]. In QSARINS the prediction and training data sets were generated by total data set division through random selection (20 % test). QSARINS default settings was to construct GA-MLR-based QSAR model and q2 function was used for GA maximization [18]. For avoiding of overfit, the selection of molecular MDs was limited to 4 MDs and all models were validated, randomized and analyzed for AD. The various methods were used for QSAR models quality and validation check several methods were used [19].

RESULTS AND DISCUSSION

Molecular docking analysis: The MDA was performed to determine the binding affinity of NCAs to SARS-CoV-2 spike protein N-terminal domain (PDB: 7B62), SARS-CoV-2 nucleocapsid protein C-terminal domain (PDB: 7UXZ), SARS-CoV-2 main protease (PDB: 7DGB) and SARS-CoV-2 3CL protease (PDB: 7P35) binding site. The MDA scores of all synthesized compounds are given in Table-1. All compounds strongly inhibited by completely occupying active sites in target protein. Among all compounds, compound **5d** was found to be most potent when docked with SARS-CoV-2 nucleocapsid protein C-terminal domain (PDB: 7UXZ) and SARS-CoV-2 main protease (PDB: 7DGB); whereas compound **5e** was found to be most potent when docked with SARS-CoV-2 spike protein N-terminal domain (7B62) and SARS-CoV-2 3CL protease (PDB: 7P35) as exhibited the highest binding affinity. Compound **5d** demonstrated favourable orientation within SARS-CoV-2 nucleocapsid protein C-terminal domain (PDB: 7UXZ), SARS-CoV-2 main protease (PDB: 7DGB) binding sites; whereas compound **5e** exhibited favourable orientation within the SARS-CoV-2 spike protein N-terminal domain (7B62) and SARS-CoV-2 3CL protease (PDB: 7P35). Based on the MDA data of compound **5e** with 7B62 (Fig. 1), it is revealed that the 2D structure of compound **5e** underwent significant interactions with the amino acids of SARS-CoV-2 spike protein N-terminal domain. Specifically, the conventional hydrogen bonds are formed between the oxygen atom of the chromene nucleus or benzopyran ring of compound **5e** and the tyrosine amino acid of protein 7B62. Hydrogen bond interactions are also observed between the nitro group of compound **5e** and the serine amino acid of the protein. Furthermore, the 3D representation of MDA complex assures presence of such interactions, providing more details about binding mode of compound **5e** within the active site of the SARS-CoV-2 spike protein N-terminal domain (Fig. 1). The hydrogen bonding between the ligand (compound **5e**) and the protein residues (tyrosine and serine amino acids) stabilizes the complex and enhances its binding affinity [6].

The H-bond pose in Fig. 1 illustrates the precise orientation of compound **5e** within the binding site of protein, highlighting the specific hydrogen bond interactions between the ligand

TABLE-1
DOCKING SCORES OF 18 COMPOUNDS AND CONTROLS

Ligand	Binding affinity (with 7B62)	Ligand	Binding affinity (with 7UXZ)	Ligand	Binding affinity (with 7DGB)	Ligand	Binding affinity (with 7P35)
5e	-9.1	**5d**	-7.5	**5d**	-8.7	**5e**	-8.4
6d	-8.9	**6c**	-7.5	**4d**	-8.6	**5d**	-8.0
6c	-8.8	**6d**	-7.5	**5b**	-8.6	**5a**	-7.9
6e	-8.8	**6e**	-7.5	**6d**	-8.6	**5b**	-7.9
6b	-8.6	**4c**	-7.4	**5e**	-8.5	**6a**	-7.7
6a	-8.5	**6b**	-7.4	**6b**	-8.5	**6e**	-7.7
Biliverdin	-8.5	**4b**	-7.3	**6a**	-8.4	**5c**	-7.5
4e	-8.3	**4e**	-7.3	**6c**	-8.4	**6b**	-7.5
4b	-8.1	**5a**	-7.3	**6e**	-8.4	**4a**	-7.3
5c	-8.1	**5b**	-7.3	**4a**	-8.3	**4d**	-7.3
4d	-7.9	**6a**	-7.2	**5a**	-8.2	**6c**	-7.3
5a	-7.9	**4d**	-7.1	**5c**	-8.1	**6d**	-7.3
5b	-7.8	**4a**	-7.0	**4b**	-7.9	**4e**	-7.1
5d	-7.8	**5c**	-7.0	**4e**	-7.8	Rupintrivir	-7.1
4a	-7.7	**5e**	-6.6	**4c**	-7.7	**4b**	-6.4
4c	-7.7	Chicoric acid	-6.4	**3**	-7.1	**4c**	-6.0
3	-6.8	**3**	-6.2	Penatanamide	-6.8	**3**	-5.8
2	-6.3	**2**	-5.9	**2**	-6.5	**2**	-5.5
1	-5.9	**1**	-5.6	**1**	-5.8	**1**	-4.9

Note: The results are shown for 19 ligands in the table.

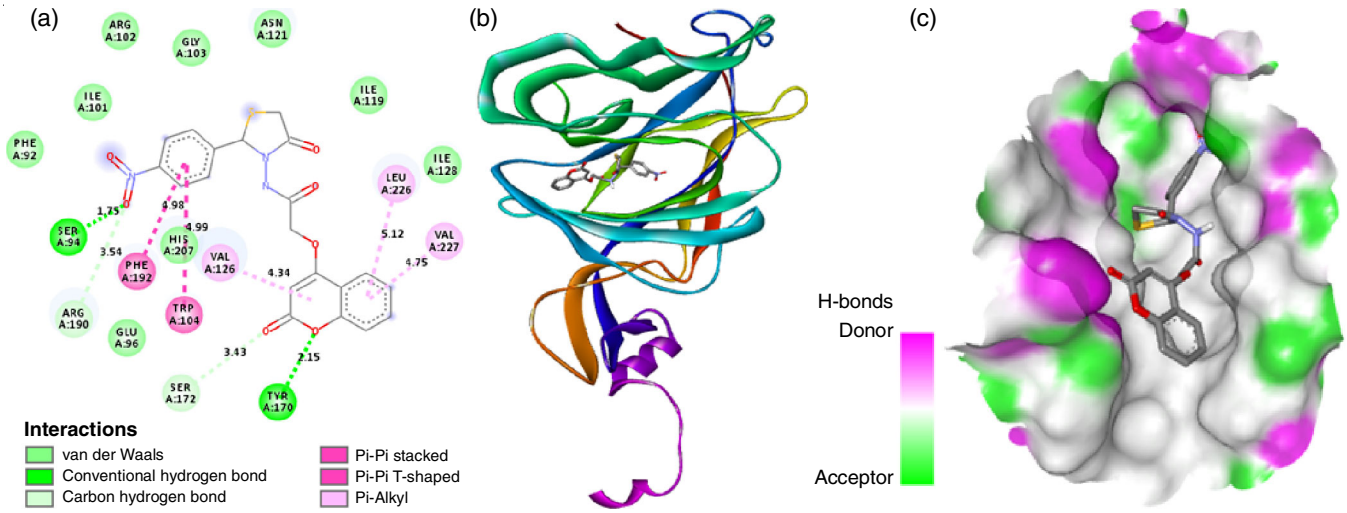

Fig. 1. (a) 2D dock image of compound **5e** with 7B62 (S), (b) 3D dock image for compound **5e** with 7B62 (S), (c) H bond pose for compound **5e** with 7B62

and the protein residues. The significance of these interactions lies in the potential of compound **5e** to disrupt the function of the SARS-CoV-2 spike protein, particularly the N-terminal domain, which is crucial for the viral entry and infection [20]. By forming the hydrogen bonds with key amino acids in the protein, compound **5e** may hinder the virus's ability to bind to host cells and thereby reduce viral infectivity. The 2D structure of compound **5e** reveals interaction with specific amino acids of SARS-CoV-2 3CL protease. Remarkably, the conventional hydrogen bonds are formed between the carbonyl group present on the chromene nucleus of compound **5e** and the glycine and cysteine amino acids of protein (Fig. 2). These interactions are important to stabilize ligand-protein complex (LPC) and enhance its binding affinity. The MDA complex 3D representation confirms presence of such interactions and suggests how compound **5e** fits in SARS-CoV-2 3CL protease active site (Fig. 2).

The H-bond pose in Fig. 2 illustrates the precise orientation of compound **5e** within the binding site of 3CL protease, highlighting the specific hydrogen bond interactions between the ligand and the glycine and cysteine amino acids of the protein (Fig. 2). Similar to the previously reported study [21], here, the molecular interaction between ligand and the proteins revealed compound **5e** to inhibit the activity of the SARS-CoV-2 3CL protease, which is essential for the virus's replication process. By forming hydrogen bonds with key amino acids in the active site of enzyme, compound **5e** may interfere with the protease's function, ultimately hindering viral replication and spread. The 2D structure of compound **5d** reveals the hydrogen bond interactions with specific amino acids of SARS-CoV-2 nucleocapsid

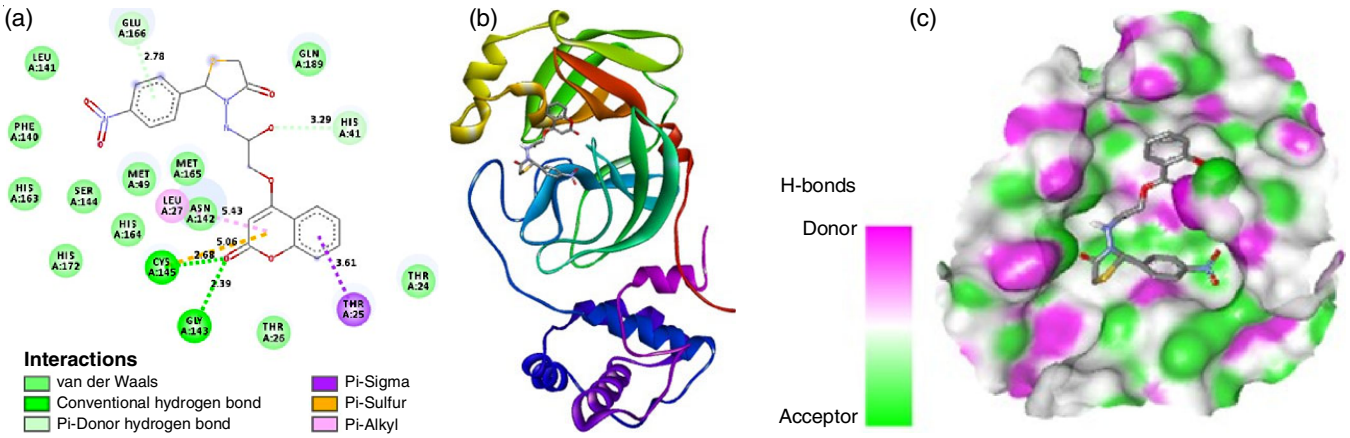

Fig. 2. (a) 2D dock image for compound **5e** with 7P35 (3CL), (b) 2D dock image for compound **5e** with 7P35 (3CL), (c) 3D dock image for compound **5e** with 7P35 (3CL)

protein C-terminal domain. The carbonyl group present on the chromene nucleus of compound **5d** forms a hydrogen bond with the asparagine amino acid in the protein. Additionally, another hydrogen bond interaction is observed between the nitro group and the arginine amino acid of the protein (Fig. 3). These interactions play a crucial role to stabilize ligand-protein complex (LPC) and enhance its binding affinity. The 3D representation of MDA complex also determines presence of such interactions. The hydrogen bond interactions between the ligand and the specific amino acids in the protein are essential for the ligand's optimal binding (Fig. 3).

The H-bond pose in the figure illustrates the precise orientation of compound **5d** within the binding site of the nucleocapsid protein (Fig. 3). As previously observed [22], in present study, the molecular interactions show the potential of compound **5d** to interfere with the function of SARS-CoV-2 nucleocapsid protein, particularly the C-terminal domain. Since nucleocapsid protein is involved in viral RNA binding and plays an important role in viral replication & packaging [23], by forming hydrogen bonds with key amino acids in the protein, compound **5d** may disrupt the protein's function and inhibit viral replication and assembly. Furthermore, the 2D structure of compound **5d** reveals significant hydrogen bond interactions with specific amino acids of the SARS-CoV-2 main protease. The carbonyl group present on the chromene nucleus of compound **5d** forms a hydrogen bond with the arginine amino acid in the protein. Additionally, another hydrogen bond interaction is observed between the nitro group of compound **5d** and the glutamine amino acid of protein (Fig. 4). Moreover, there is an interaction between the carbonyl group present on the aldehyde benzene ring of compound **5d** and the glycine amino acid of protein. The 3D representation shows hydrogen bond interactions between the ligand and the specific amino acids in the protein are essential for the ligand's optimal binding (Fig. 4).

These interactions demonstrate the potential of compound **5d** to interfere with the function of SARS-CoV-2 main protease. The main protease is essential for viral replication and is considered a promising target for antiviral drugs [24]. By forming hydrogen bonds with key amino acids in the protein, compound **5d** may disrupt the protease's function and inhibit viral replication and spread.

The variation in antiviral activity observed among NCA derivatives can be attributed to differences in their molecular structures and interactions with the target viral proteins. MDA provided valuable insights into the potential binding interactions between compound **5e** and the SARS-CoV-2 spike protein *N*-terminal domain. Nevertheless, it is crucial to validate these findings through experimental studies, while MDA offers valuable initial insights, *in vitro* and *in vivo* experiments are essential for confirming the actual binding affinity and antiviral efficacy of these compounds.

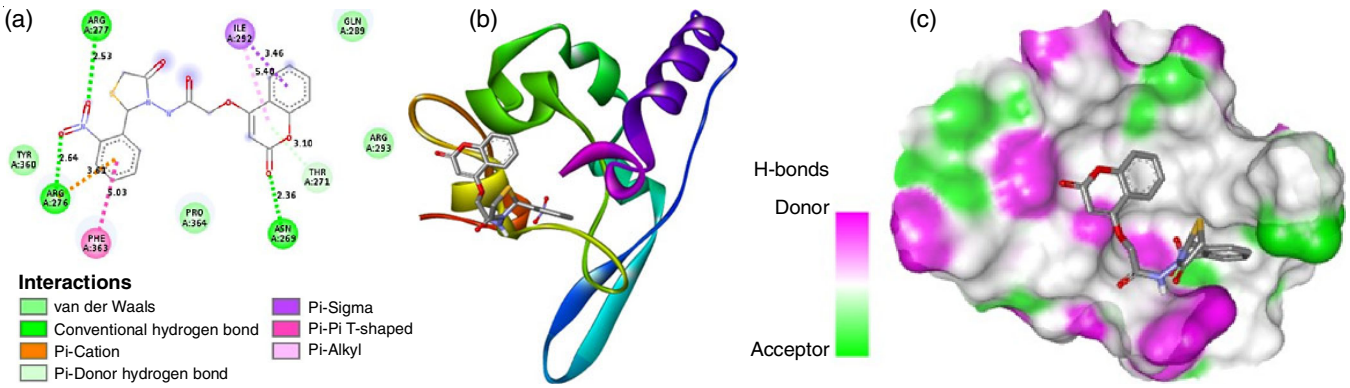

Fig. 3. (a) 2D dock image for compound **5d** with 7UXZ (N), (b) 3D dock image for compound **5d** with 7UXZ (N), (c) H bond pose for compound **5d** with 7UXZ (N)

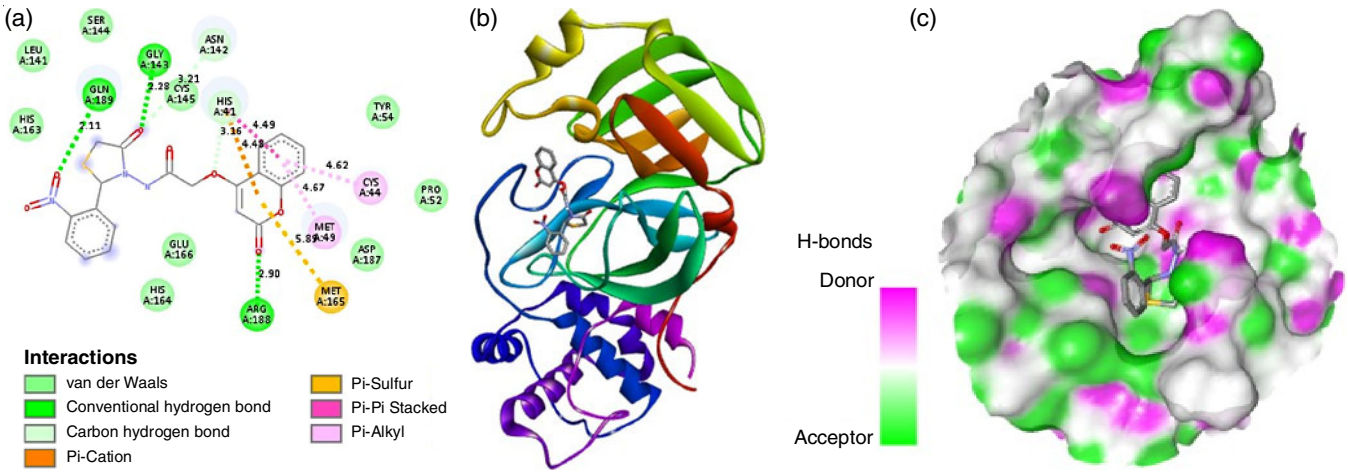

Fig. 4. (a) 2D dock image for compound **5d** with 7DGB (mPro), (b) 3D dock image for compound **5d** with 7DGB (mPro), (c) H bond pose for compound **5d** with 7DGB (mPro)

QSAR analysis: For the QSAR analysis, the NCAs and their inhibition activity (pIC_{50}) were used as the primary data. The present study generated several QSAR models using QSARINS, but here only models 1, 2 and 3 are discussed. The MLR method was used for obtaining models. Table-2 presents parameters for model 1, 2 and 3; whereas parameters involved in Table-3 presents selected models 1, 2 and 3. Symbols expansion and meaning were previously reported [19].

Model 1:

pIC_{50} = -0.0743 (± 0.0248) VR2_Dzs – 0.5889 (± 0.1657) PubchemFP12 + 3.8306 (± 0.2665); n = 18 (1)

Model 2:

pIC_{50} = -0.1062 (± 0.0284) VR2_Dzs – 0.5814 (± 0.1679) MLFER_S + 2.705 (± 0.4994); n = 18 (2)

Model 3:

pIC_{50} = -0.4911 (± 0.1796) MDEN-23 – 0.704 (± 0.1893) PubchemFP12 + 3.1755 (± 0.1631); n = 18 (3)

Model 4:

pCC_{50} = 0.0748 (± 0.0215) AATSC6v – 1.8665 (± 0.4944) AATSC6s + 2.1426 (± 0.2139); n = 18 (4)

The data given in Table-2 presents the variables involved in selected model 1, 2, 3 and 4; Table-4 presents estimated and predicted inhibition activities (pIC_{50}) for models 1, 2 & 3; and Table-3 presents CC_{50} of model 4, whereas Figs. 5 and 6 illustrates the regression and correlation of experimental & predictive inhibition and CC_{50} of NCAs (**1-18**).

The applicability domain (AD) of generated model was determined with William's plot and was established in squared area of ± 3 standard residues and leverage threshold h* = 0.6 for all models 1, 2 and 3 (h* = 3p'/n, where p' is parameters number in model+1, n is compounds number). Williams plot (Fig. 5) for models 1, 2 and 3 exhibited one outlier in model 1 and 2, but there is no outlier in model 3. Hence, the correlation between MDs for 2D-QSAR model 3, is given in Table-3.

In present study, the 2D QSAR analysis was conducted on NCAs and only three models *i.e.*, models 1, 2 and 3 were selected.

TABLE-2
STATISTICAL PARAMETERS FOR DEVELOPED MODELS 1, 2, 3 AND 4

	Threshold value	Model 1	Model 2	Model 3	Model 4
R2	> 0.6	0.8805	0.8751	0.8627	0.8913
s	< 0.3	0.8606	0.1009	0.1058	0.1427
R2adj	> 0.6	0.0988	0.8543	0.8398	0.8716
R2-R2adj	< 0.3	0.0199	0.0208	0.0229	0.0198
CCC tr	> 0.85	0.9364	0.9334	0.9263	0.9425
F	Higher than the theoretical value	44.2018	42.0420	37.6974	45.1147
Q2loo (r2CV)	> 0.5	0.8186	0.8196	0.8152	0.7927
R2- Q2loo	< 0.3	0.0619	0.0555	0.0475	0.0986
Q2lmo	> 0.5	0.7957	0.7584	0.7914	0.7702
R2Yscr	<R2 (smallest is better)	0.1418	0.1435	0.1425	0.1537
LOO					
r2m	> 0.5	0.7828	0.8121	0.7930	0.7322
r'2m	> 0.5	0.7029	0.6669	0.6777	0.7085
k'	0.85 < k or k' < 1.15	0.9988	1.0002	0.9988	1.0031
k	0.85 < k or k' < 1.15	1.0003	0.9989	1.0003	0.9930
r2-r20/r2	< 0.1	0.0026	0.0001	0.0010	0.0085
r2-r'20/r2	< 0.1	0.0251	0.0425	0.0352	0.0034

*Values in parenthesis in equation are in 95% confidence interval values.

TABLE-3
PARAMETERS FOR MODEL 1, 2, 3 AND 4 FOR THE GIVEN DESIGNED COMPOUNDS

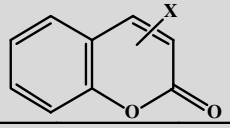

Compd. ID	Compound with substituent X	VR2_Dzs	Pubchem FP12	MLFER_S	MDEN-23	AATSC6v	AATSC6s
1	OH	6.689	0	2.093	0.000	8.965982	-0.82836
2	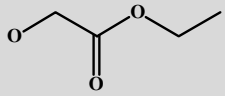	8.014	0	2.387	0.000	4.631205	-0.60027
3	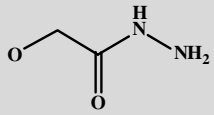	9.631	0	2.575	0.000	-8.51681	-0.78718
4a	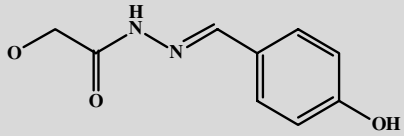	7.422	1	3.399	0.000	-1.91256	-0.45303
4b	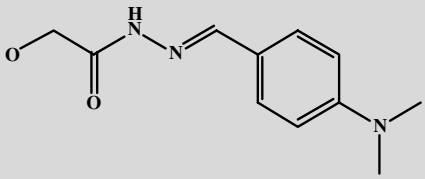	11.307	1	3.297	0.309	5.247799	-0.16823
4c	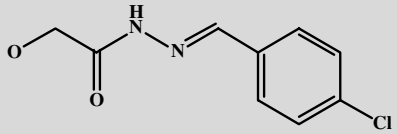	7.524	1	3.234	0.000	-1.41793	-0.42702
4d	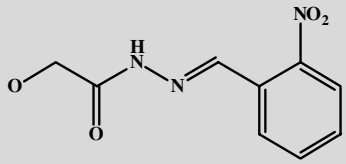	8.167	1	3.291	0.447	-0.09458	-0.6072
4e	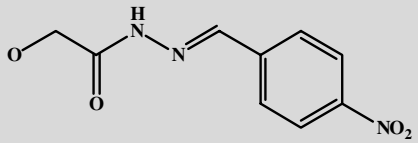	10.168	1	3.291	0.309	-0.7543	-0.48049
5a	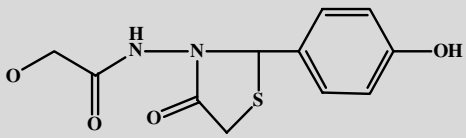	13.983	1	3.82	1.000	-5.4261	-0.529
5b	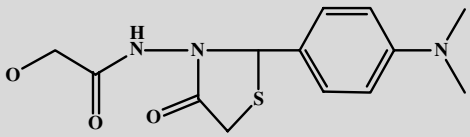	13.044	1	3.718	0.756	0.298923	-0.22747
5c	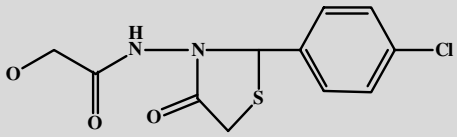	13.020	1	3.655	1.000	-4.05476	-0.40137
5d	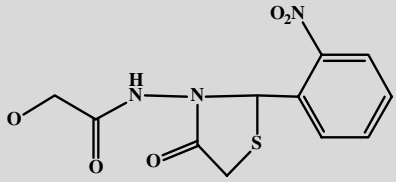	11.579	1	3.712	0.894	-6.31298	-0.58547

5e	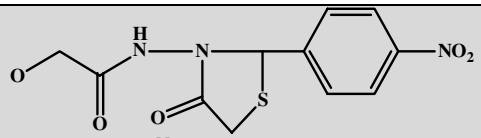	12.346	1	3.712	0.756	-4.37243	-0.52588
6a	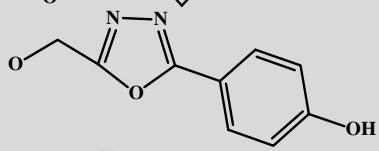	7.916	1	3.566	0.000	-6.27177	-0.26502
6b	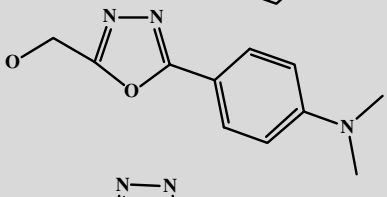	8.192	1	3.464	0.309	3.659747	-0.17268
6c	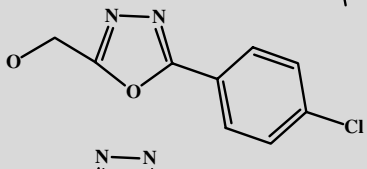	7.754	1	3.401	0.000	-4.99272	-0.45286
6d	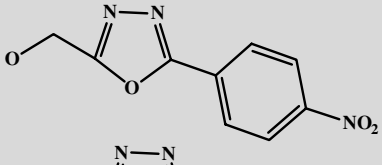	8.049	1	3.458	0.309	-5.10706	-0.50784
6e	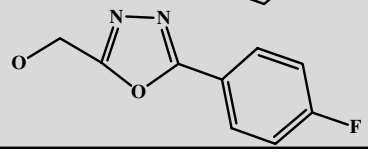	7.930	1	3.319	0.000	-5.3152	-0.21173

TABLE-4
CALCULATED AND PREDICTED INHIBITION ACTIVITIES (pIC_{50}) BY MODELS 1, 2 & 3 AND CC_{50} BY MODEL 4

Compd.	pIC_{50}	Model 1		Model 2		Model 3		pCC_{50}	Model 4	
		Cal	LOO	Cal	LOO	Cal	LOO		Cal	LOO
2	3.139	3.3339	–	3.2112	–	3.1755	–	3.266	3.6095	3.7773
3	3.194	3.2355	3.2785	3.2415	3.2894	3.1755	3.1570	3.428	2.9745	2.9806
4a	3.157	3.1155	3.0725	3.1790	3.1942	3.1755	3.1940	2.964	2.8450	–
4b	3.932	3.8684	3.8563	3.8928	3.8847	3.8795	3.8685	3.004	2.8492	2.8273
4c	3.572	3.5799	3.5809	3.4207	3.4010	3.7279	3.7419	2.893	2.8335	2.8319
4d	3.939	3.8608	3.8467	3.7860	3.7623	3.8795	3.8670	2.853	3.2688	3.2547
4e	3.708	3.8131	3.8271	3.7508	3.7557	3.6599	3.6558	3.322	2.9829	–
5a	3.570	3.6645	3.6725	3.5382	3.5357	3.7279	3.7420	3.080	2.7239	2.7038
5b	3.499	3.3812	3.3315	3.4405	3.4147	3.3884	3.3420	2.882	2.5895	2.5550
5c	3.449	3.4510	3.4515	3.4810	3.4896	3.5083	3.5190	2.774	2.5883	2.5715
5d	3.311	3.4528	3.4893	3.4469	3.4818	3.3884	3.4209	2.756	2.7629	2.7598
5e	3.541	3.5597	–	3.6331	–	3.4402	–	2.781	2.7969	2.8024
6a	3.562	3.5028	3.4919	3.5516	3.5496	3.5083	3.4985	2.745	2.1679	2.2791
6b	3.914	3.8317	3.8194	3.9374	3.9428	3.8795	3.8723	1.865	2.7387	2.7586
6c	3.936	3.8112	3.7948	3.8487	3.8354	3.7279	3.7094	2.684	2.6142	–
6d	3.821	3.8437	3.8474	3.8586	3.8650	3.8795	3.8918	2.736	2.7083	2.7114
6e	3.670	3.8218	3.8431	3.8604	3.8913	3.7279	3.7331	2.681	2.1400	2.1465

Models 1, 2 and 3 included VR2.Dzs, MLFR_S, MDEN-2, PubChemFP12, AATSC6v and AATSC6s as the MDs. The descriptor VR2.Dzs is defined as 2D type normalized Randic-type eigenvector-based index from Barysz matrix/weighted by I-state [25]; the descriptor MLFR_S is defined as molecular linear free energy relation descriptor to quantify dipolarity/polarizability; the descriptor MDEN-2 is defined molecular distance edge between all secondary and tertiary nitrogen's [26]; PubChemFP12 fingerprint descriptor related to the number of carbon atoms is discriminative for P-gp properties [27]; the descriptor of AATSC6v is defined as average centred Broto-Moreau autocorrelation -lag 6/weighted by van der Waals [28]; whereas the descriptor AATSC6s is defined as the Average centred Broto-Moreau autocorrelation–lag6/weighted by I-state [29]. All models 1, 2 and 3 exhibited decent model fitting and fulfil OECD standard, however, for pIC_{50} among

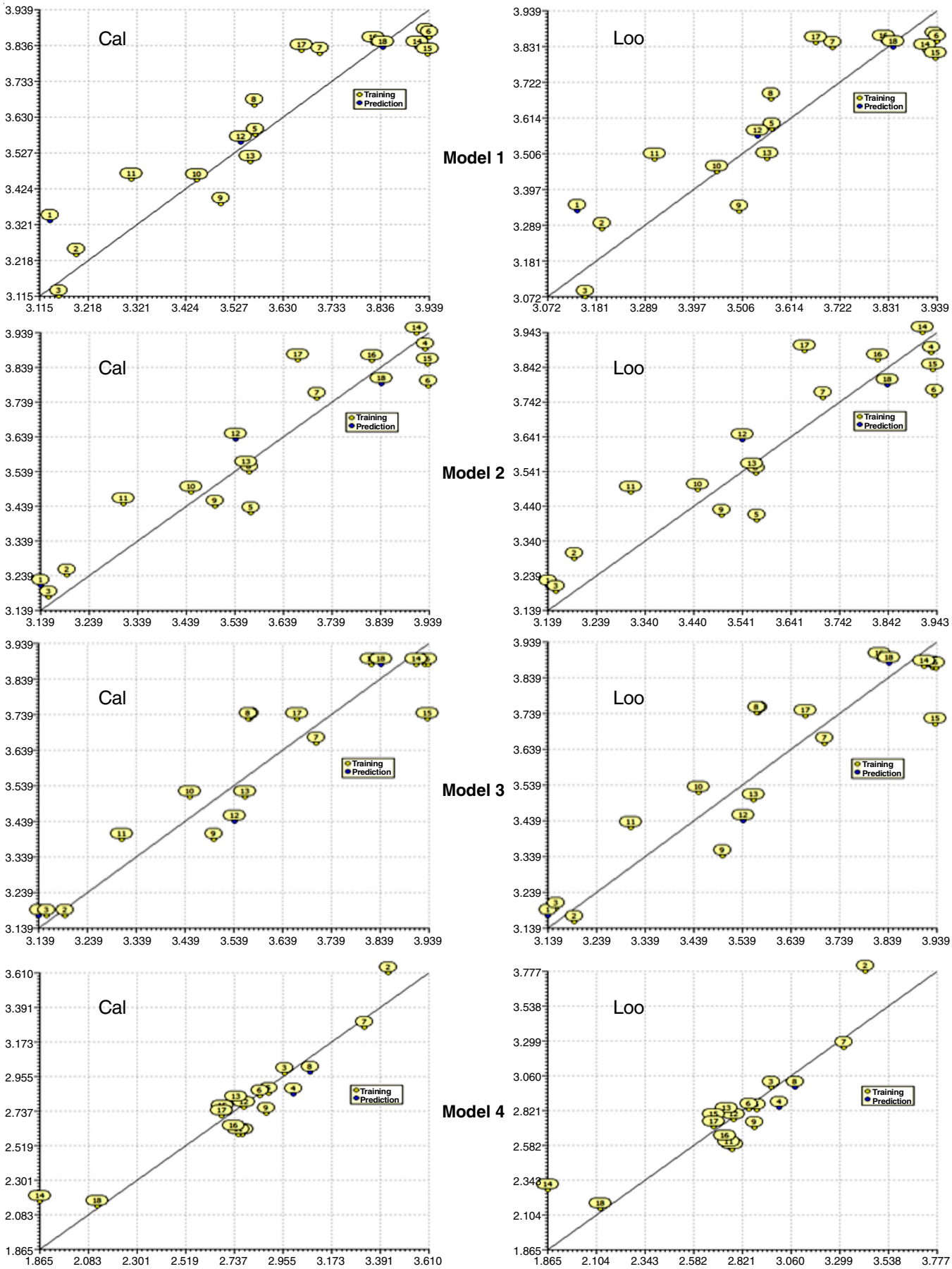

Fig. 5. Regression plots for models 1, 2, 3 and 4

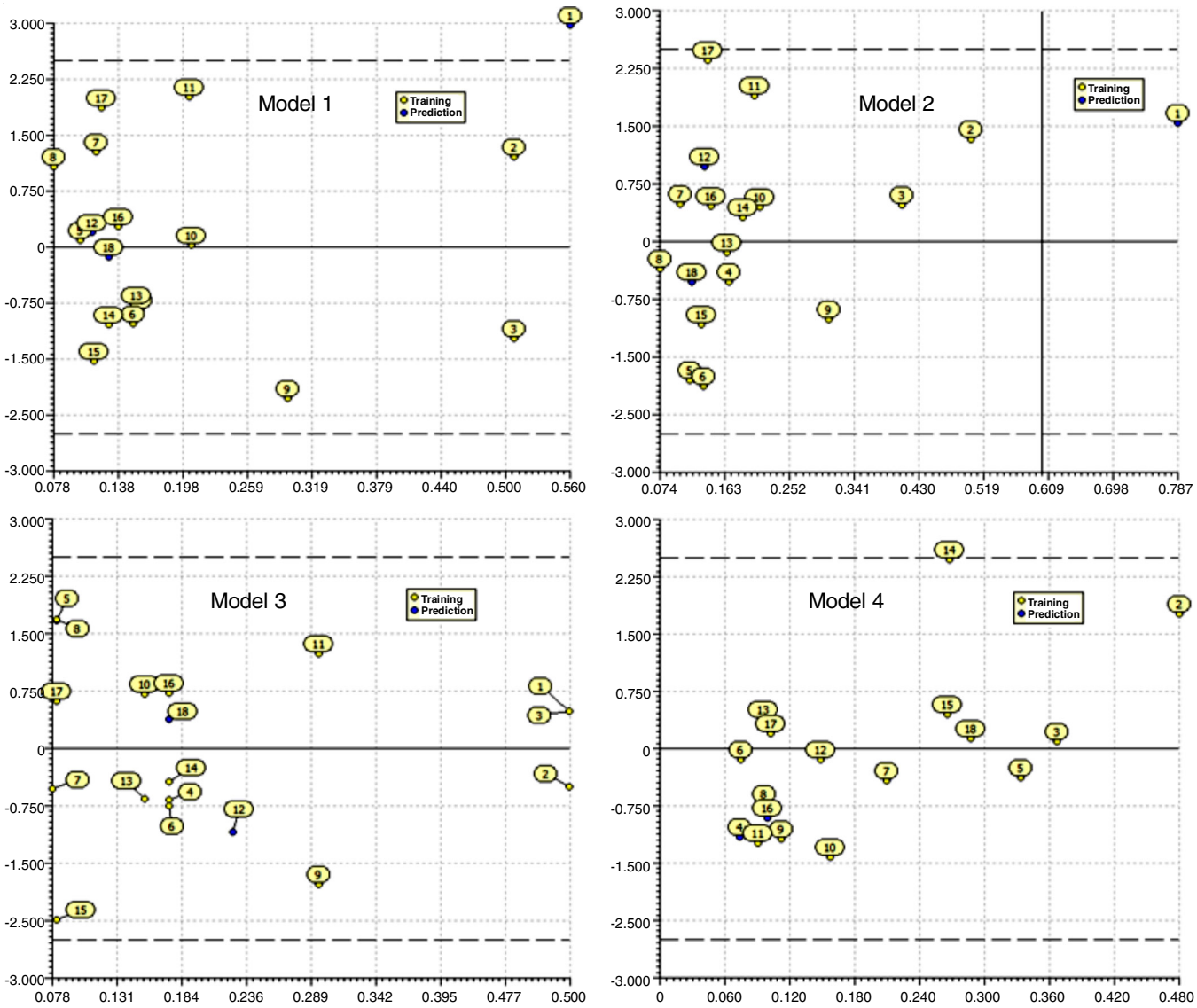

Fig. 6. Williams plot for models 1, 2, 3 and 4

models 1, 2 and 3, the QSAR model 3 was chosen as the best model based on the loo and lmo as the parameters. Also, for PCC_{50} model 4 was found to be as best fit, so selected for QSAR of NCAs for CC_{50}. Hence, model 3 could explain and predict 86.27% of inhibition variance. Model 3 showed good internal predictivity with Q2 = 0.8152. Low r2 reveals that decent result of model is not based on change correlation or training set structural dependency. Whereas model 4 could predict 89.13% of the variance of CC_{50} of NCAs. Model 4 showed good internal predictivity with Q2 = 0.7957. Low r2 reveals that decent result of model is not based on change correlation or training set structural dependency. The molecular descriptors (MDs) number significance of models was assured based on minimum difference (< 0.3) between R2 and R2 adj that was 0.0199 for model 3 and 0.0198 for model 4. Similarly, model's stability was assured based on minimum difference (< 0.3) between R2 and Q2 loo, 0.0475 in model 3 and 0.0986 in model 4. Model 3 (for pIC_{50}) and model 4 (for pCC_{50}) were significant and predictive. William's plots of model 3 showed no outlier and model 4 showed 1 outlier indicating the applicability domain (AD) of the two models. Model 3 suggests positive input of VR2.Dzs, MLFR_S, MDEN-2 and PubChemFP12 indicate that the inhibition is correlated directly to VR2.Dzs, MLFR_S, MDEN-2 and PubChemFP12. This means the inhibition activity of NCA is directly related to the normalized Randic-type eigen vector-based index, molecular linear free energy, molecular distance edge between secondary and tertiary nitrogen and fingerprint MDs [12].

The QSAR results of compounds **2-3**, **4a-e**, **5a-e** and **6a-e** when compared with compound **1**, revealed that substitution of imino and oxadiazole group with strong electron donating group such as -$N(CH_3)_2$ & -OH at *para*-position of benzene ring in compounds **4a**, **6a** & **6b**; and strong electron withdrawing group like -Cl at the *para* position of benzene ring in compound **6b** offers high inhibition activity, whereas model 4 revealed that the positive contribution of AATSC6v and AATSC6s is correlated with CC_{50} of NCAs. This means that CC_{50} of NCAs is related to the average centred Broto-Moreau

autocorrelation - lag 6/weighted by van der Waals and Average centred Broto-Moreau autocorrelation–lag6/weighted by I-state [19]. Also, the cytotoxicity study data of NCAs supports that the oxadiazole group with a strong electron donating group such as the -OH group at the *para* position of benzene ring in compound **6a**, exhibited the maximum CC_{50} or safety against normal healthy cells [30]. The QSAR study supports that compound **6a** possesses the lowest IC_{50} and maximum CC_{50} when related to VR2.Dzs, MLFR_S, MDEN-2, PubChemFP12, AATSC6v and AATSC6s MDs. The QSAR studies were carried out for novel coumarin derivatives with their anti-coronavirus activity to generate few useful QSAR models. Stability, validity, robustness and application of ideal QSAR models have been established and found comparable with OECD criteria for QSAR. All the series of NCAs (**2-3**, **4a-e**, **5a-e** and **6a-e**) offered good QSAR with coronavirus inhibition activity and cytotoxicity (CC_{50}).

Conclusion

The severity of coronavirus and the re-emergence of viruses have prompted the development of novel therapeutic strategies. The present study conducted molecular docking analysis (MDA) and and quantitative structure-activity relationship (QSAR) analysis on novel coumarin analogues (NCAs) against coronaviruses, revealing promising insights into their mechanisms of action and QSAR. The MDA particularly on compound **5e**, demonstrated potential binding interactions with the SARS-CoV-2 spike protein N-terminal domain, suggesting a probable mechanism of action. However, the experimental validation is crucial to confirm these findings. Additionally, the QSAR studies identified several molecular descriptors (VR2.Dzs, MLFR_S, MDEN-2, PubChemFP12, AATSC6v and AATSC6s) as significant contributors to coronavirus inhibition activity and cytotoxicity (CC_{50}). Robust QSAR models were developed, meeting OECD criteria, indicating their stability, validity and applicability. All series of NCAs exhibited favourable QSAR profiles, indicating their potential as antiviral agents against coronaviruses. The protocol and pattern of present study results were also supported by other studies. Overall, the findings demonstrated the potential of NCAs as antiviral candidates, warranting further preclinical and clinical investigations. While MDA provides initial insights, validation through *in vitro* and *in vivo* experiments is imperative. Nonetheless, these results provide a solid foundation for the development of novel therapeutics to combat coronavirus infections.

ACKNOWLEDGEMENTS

The authors thank the Ministry of Higher Education (Ref: FRGS/1/2020/STG01/AIMST/01/1) and AIMST University for financial support and assistance in completing this study.

CONFLICT OF INTEREST

The authors declare that there is no conflict of interests regarding the publication of this article.

REFERENCES

1. S. Mishra, A. Pandey and S. Manvati, *Heliyon*, **6**, e03217 (2020); https://doi.org/10.1016/j.heliyon.2020.e03217
2. D. Gupta, E. Guliani and K. Bajaj, *Top. Curr. Chem.(Z)*, **382**, 16 (2024); https://doi.org/10.1007/s41061-024-00462-z
3. E.K. Akkol, Y. Genç, B. Karpuz, E. Sobarzo-Sánchez and R. Capasso, *Cancers*, **12**, 1959 (2020); https://doi.org/10.3390/cancers12071959
4. G. Salgado-Moran, Wilson Cardona V., L. Gerli-Candia, L.H. Mendoza-Huizar and T. Abdizadeh, *J. Chil. Chem. Soc.*, **67**, 5521 (2022); https://doi.org/10.4067/S0717-97072022000205521
5. M. Özdemir, B. Köksoy, D. Ceyhan, K. Sayin, E. Erçag, M. Bulut and B. Yalçin, *J. Biomol. Struct. Dyn.*, **40**, 4905 (2022); https://doi.org/10.1080/07391102.2020.1863263
6. D.A. Milenkovic, D.S. Dimic, E.H. Avdovic and Z.S. Markovic, *RSC Adv.*, **10**, 35099 (2020); https://doi.org/10.1039/D0RA07062A
7. Y. Peng, N. Du, Y. Lei, S. Dorje, J. Qi, T. Luo, G.F. Gao and H. Song, *EMBO J.*, **39**, e105938 (2020); https://doi.org/10.15252/embj.2020105938
8. S.M. Patil, R.M. Martiz, R. Ramu, P.S. Shirahatti, A. Prakash, J. Chandra S and V.L. Ranganatha, *J. Biomol. Struct. Dyn.*, **40**, 13032 (2022); https://doi.org/10.1080/07391102.2021.1978322
9. U.R. Abdelmohsen, A. Albohy, B.S. Abdulrazik, S.A. Bayoumi, L.G. Malak, I.S. Khallaf, G. Bringmann and S.F. Farag, *RSC Adv.*, **11**, 16970 (2021); https://doi.org/10.1039/D1RA01989A
10. A.T. McNutt, P. Francoeur, R. Aggarwal, T. Masuda, R. Meli, M. Ragoza, J. Sunseri and D.R. Koes, *J. Cheminform.*, **13**, 43 (2021); https://doi.org/10.1186/s13321-021-00522-2
11. Z.M. Alamshany, R.R. Khattab, N.A. Hassan, A.A. El-Sayed, M.A. Tantawy, A. Mostafa and A.A. Hassan, *Molecules*, **28**, 739 (2023); https://doi.org/10.3390/molecules28020739
12. R. Veerasamy and R. Karunakaran, *J. Genet. Eng. Biotechnol.*, **20**, 58 (2022); https://doi.org/10.1186/s43141-022-00339-y
13. M. Shaharyar, A. Mazumder, Salahuddin, R. Garg and R.D. Pandey, *Arab. J. Chem.*, **9**, S342 (2016); https://doi.org/10.1016/j.arabjc.2011.04.013
14. M.M. Varshney, A. Husain and V. Parcha, *Med. Chem. Res.*, **23**, 4034 (2014); https://doi.org/10.1007/s00044-014-0982-4
15. S. Sahin and N. Dege, *Iran. J. Chem. Chem. Eng.*, **42**, 2451 (2023); https://doi.org/10.30492/IJCCE.2022.559865.5508
16. H.Z. Naji and E.M. Hussain, *Bionatura*, **8**, 1 (2023); https://doi.org/10.21931/RB/CSS/2023.08.03.20
17. Z. Amer and E.O. Al-Tamimi, *History of Medicine*, **9**, 1205 (2023); https://doi.org/10.17720/2409-5834.v9.1.2023.143
18. P. Gramatica, On the Development and Validation of QSAR Models, In: Methods in Molecular Biology, Clifton: N.J., pp. 499–526 (2013).
19. R. Veerasamy, H. Rajak, A. Jain, S. Sivadasan, P.V. Christapher and R. Agrawal, *Int. J. Drug Design Discov.*, **2**, 511 (2011).
20. Y. Lv, S. Ge, Q. Zhu, M. Si, C. Wang and H. He, *New J. Chem.*, **47**, 2651 (2023); https://doi.org/10.1039/D2NJ05019F
21. R. Abdizadeh, F. Hadizadeh and T. Abdizadeh, *Mol. Divers.*, **26**, 1053 (2022); https://doi.org/10.1007/s11030-021-10230-6
22. A. Pohler, S. Abdelfatah, M. Riedl, C. Meesters, A. Hildebrandt and T. Efferth, *Pharmaceuticals*, **15**, 1046 (2022); https://doi.org/10.3390/ph15091046
23. Y. Wang, X. Ling, C. Zhang, J. Zou, B. Luo, Y. Luo, X. Jia, G. Jia, M. Zhang, J. Hu, T. Liu, Y. Wang, K. Lu, D. Li, J. Ma, C. Liu and Z. Su, *Mol. Biomed.*, **4**, 16 (2023); https://doi.org/10.1186/s43556-023-00129-z
24. M. Roney, G. Singh, A.K.M.M. Huq, M.S. Forid, W.M.B.W. Ishak, K. Rullah, M.F.F.M. Aluwi and S.N. Tajuddin, *Mol. Biotechnol.*, **66**, 696 (2024); https://doi.org/10.1007/s12033-023-00667-5

25. P.R. Duchowicz, N.A. Szewczuk and A.B. Pomilio, *J. Food Sci. Technol.*, **56**, 5518 (2019); https://doi.org/10.1007/s13197-019-04024-w
26. S. Liu, C. Cao and Z. Li, *J. Chem. Inf. Comput. Sci.*, **38**, 387 (1998); https://doi.org/10.1021/ci970109z
27. N. Schaduangrat, A.A. Malik and C. Nantasenamat, *PeerJ*, **9**, e11716 (2021); https://doi.org/10.7717/peerj.11716
28. I. Èabarkapa, M. Aæimovic, L. Pezo and V. Tadiæ, *J. Mex. Chem. Soc.*, **65**, 550 (2021); https://doi.org/10.29356/jmcs.v65i4.1515
29. O. Dym, I. Xenarios, H. Ke and J. Colicelli, *Mol. Pharmacol.*, **61**, 20 (2002); https://doi.org/10.1124/mol.61.1.20
30. M.A. Sa'ad, R. Kavitha, S. Fuloria, N.K. Fuloria, M. Ravichandran and P. Lalitha, *Antibiotics*, **11**, 207 (2022); https://doi.org/10.3390/antibiotics11020207